JOURNAL OF THERMOPHYSICS AND HEAT TRANSFER
Vol. 9, No. 4, October–December 1995

Comparison of Theory with Atomic Oxygen Radiance Data from a Rocket Flight

Deborah A. Levin*
Institute for Defense Analyses, Alexandria, Virginia 22311-1772
Graham V. Candler†
University of Minnesota, Minneapolis, Minnesota 55455
L. Carl Howlett‡
Utah State University, Logan, Utah 84322-4140
and
Ellis E. Whiting§
Eloret Institute, Palo Alto, California 94303

Results obtained from a state-of-the-art flow and radiation model are compared with vacuum-ultraviolet radiance data obtained from the recent Bow Shock 2 Flight Experiment. An extensive data set of atomic-oxygen resonance radiance measurements was obtained in flight for a re-entry speed of 5 km/s between the altitudes of approximately 65–85 km. A description of the NO photoionization cell used, the data, and the interpretation of the data will be presented. A new radiation model appropriate to the flight conditions of Bow Shock 2 is proposed. Comparison of theory with the data shows that at high altitudes the flow is optically thin. At altitudes lower than about 75 km the flow is optically thick and the disagreement between theory and experiment is attributed to the inadequate treatment of photon escape mechanisms from the shock layer.

Nomenclature

A = Einstein spontaneous emission coefficient, s^{-1}
B = absorption rate, $cm^3/(erg\text{-}s^2)$
B' = stimulated emission rate, $cm^3/(erg\text{-}s^2)$
h = Planck's constant, erg-s
I_v = specific intensity, $erg/(s\text{-}sr\text{-}cm^2\text{-}Hz)$
J_v = mean intensity, $erg/(s\text{-}cm^2\text{-}Hz)$
k_f = forward rate coefficient, cm^3(/molecule-s)
k_r = reverse rate coefficient, cm^3(/molecule-s)
k_0 = absorption coefficient at the resonance wavelength, cm^{-1}
M = a neutral species, number/cm^3
n_t = total number density in the flow, number/cm^3
Q_i = electronic partition function
S_v = source function, $(erg\text{-}s/cm^3)$
γ = angle between the sensor and the effective stagnation streamline, deg
Δx = penetration distance, cm
ρ = escape factor
τ_v = optical depth
Φ_v = line absorption profile normalized to unit area, s
Ψ_v = emission line profile normalized to unit area, s

Subscript
v = frequency

Presented as Paper 93-2811 at the AIAA 28th Thermophysics Conference, Orlando, FL, July 6–9, 1993; received Sept. 8, 1994; revision received Feb. 9, 1995; accepted for publication Feb. 27, 1995.

*Research Staff Member, Science and Technology Division. Member AIAA.
†Associate Professor, Department of Mechanical and Aerospace Engineering. Member AIAA.
‡Technical Program Manager, Center for Space Engineering. Member AIAA.
§Member AIAA.

Introduction

THE first bow shock flight experiment (April 1990) measured the uv radiation from shock-heated gas in the nose region of a 0.1016-m nose radius rocket traveling at 3.5 km/s at altitudes from 40 to 70 km. Papers providing details on the instrumentation[1] and analyses of results[2] for the uv sensors have been presented. The second bow shock flight experiment (February 1991) provided similar types of uv data for re-entry at 5 km/s between the altitudes of about 100 to 65 km.[3,4] Recent shock-tube measurements have also been made by Sharma and Whiting[5] under velocity and number density conditions similar to the lower altitude portion of the second flight. The vacuum-ultraviolet data (VUV) obtained from the resonance atomic oxygen transition at 130.4 nm during the second flight is examined in this article. The reduction of this data was complicated by vehicle precession during re-entry caused by incomplete second stage separation. Use of navigational data has permitted the correlation of sensor-stagnation streamline angle as a function of time.[3] The data was collected over a sufficiently large spread in altitudes such that the optical thickness of the measurements varies.

Early in the re-entry (high altitudes) the atomic oxygen concentration in the shock layer may be sufficiently low such that at the resonance radiation wavelength the shock layer is optically thin. In this case the radiation obtained is directly proportional to the amount of atomic oxygen in the flow. The degree to which theory can match the density dependence of the data indicates the fidelity of the flow thermochemical modeling. For example, atomic oxygen colliding with N_2 is the precursor process to the formation of NO for the flight conditions of the bow shock flight experiments. The poor agreement between theory and experiment for the 230-nm NO radiation, particularly at altitudes above 80 km, has been reported.[4] Since the kinetic processes of NO and O are closely coupled, it is unlikely that a correct flow solution will be obtained unless both the 230 and 130.4 nm radiation data sets can be modeled.

Later in the re-entry (lower altitudes) the atomic oxygen concentration increases so that self-absorption becomes sig-

nificant. For these conditions the magnitude of the path-averaged resonance radiation is affected by the absorption in the denser, cooler boundary layer. Hence, fidelity of the shock-layer modeling of the spatial O concentration and temperature is less important. Instead it was found that the degree to which resonance emitted photons can escape from the shock-layer is crucial in obtaining agreement between theory and experiment.

The key assumptions of the radiation model that have been developed to analyze these data are summarized as follows. Excitation of atomic oxygen to the ^3S resonance state is achieved by collisions with neutral species rather than electrons. Measurements or calculations of this rate have not been made to date; hence, an estimate for the key collision rate is used. Steady state for the upper state population is assumed. The derived density functional form for the atomic oxygen radiation is compared with the atomic oxygen and NO-230 nm radiation data. It is also shown that the collision rate is sufficiently low such that the coupling of the radiation field to the electronic state rate equations is important. Self-absorption of 130.4-nm atomic oxygen resonance radiation is treated by classical radiative transport theory. The NEQAIR 2 model[6] modified to incorporate the neutral excitation mechanism was the analytic tool used to compute the resonance radiation.

Experimental Setup

VUV measurements were taken during the first and second bow shock flights. Atomic oxygen 130.4-nm radiation measurements were made with an NO-filled, CaF_2 window ionization chamber located in the stagnation region of the rocket. Due to the quartz window spectral cutoff, the sensor diode was sealed directly to the inside of the payload dome and viewed the ionized gas through a small hole of 0.5 mm diameter. The VUV gas diode was compared against a National Bureau of Standards calibrated VUV diode to yield an absolute calibration for the 130.4-nm radiation measurement. Due to out-of-band telemetry interference with the photoionization cell electronics, no data was obtained for the first flight. Major design changes to the preamplifiers from the first flight permitted data to be obtained during the second flight from 85 to 65 km altitudes. Figure 1 shows the cell and its geometry relative to the rocket payload axis. Figure 2

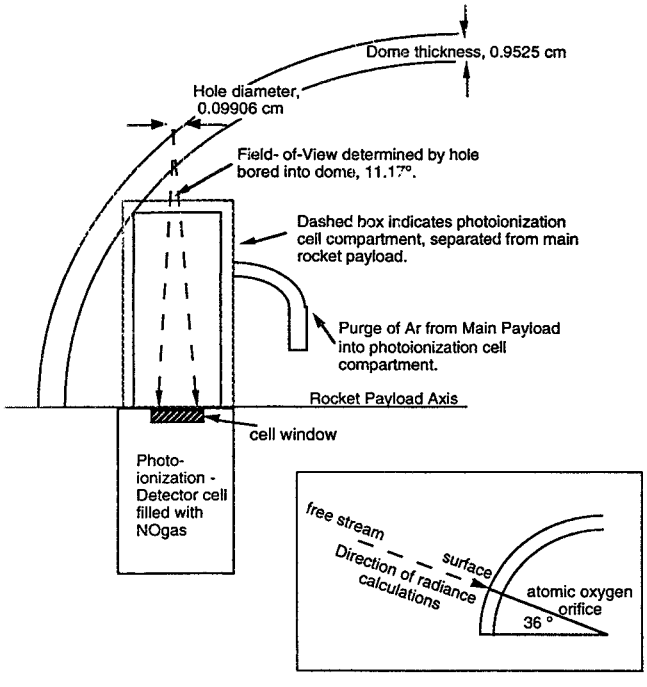

Fig. 1 NO photoionization cell used to measure atomic oxygen radiation. Drawing not to scale.

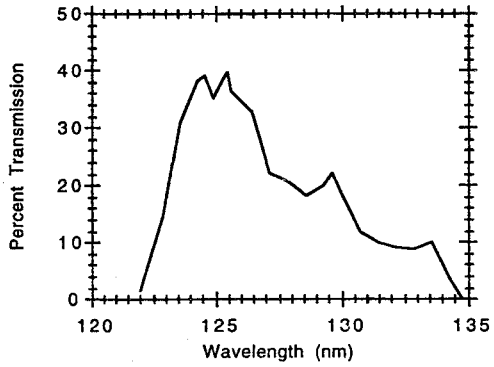

Fig. 2 Combined spectral response of the CaF_2 cell window and the NO photoionization cell.

shows the combined spectral response of the CaF_2 window and the NO-filled photoionization cell.[7]

The spectral response on the short wavelength side is limited by the transmission of the window material and on the long wavelength side by the photoionization threshold of the filling gas. If the source is sufficiently bright outside of this spectral bandwidth of the cell, the signal from the photoelectric effects from the metallic walls and the center conductor could add to the atomic resonance signal. Of primary concern is the shock-heated radiation at 230 nm since the walls of the photoionization cell are made of copper, a material with a significant work function at wavelengths shorter than 264 nm. Laboratory tests with a calibrated lamp illumination source applied to a photoionization cell similar to that flown in flight showed that the instrument output signal is totally dependent on the in-band signal.

The probable error in the absolute in-band radiance data is a function of signal level. When the important, independent sources of error are combined we estimate the accuracy of the data to be ± 38 to $\pm 45\%$ at the high-to-low signal levels, respectively. The sources of error included in this estimate are errors accumulated during the calibration procedure such as the NIST standard diode, stability of the oxygen resonance lamp, geometric factors that define the detector field of view (FOV), the precision of the dome aperture, and scattered light in the monochrometer. Electronic errors, including noise, are a function of signal level and add to the calibration error.

The photoionization cell spectral response can be seen to be much broader than the O resonance transition. The flow and radiation models (discussed below) were used to test the hypothesis that the radiation observed through this broadband filter is due to the atomic 130.4-nm triplet resonance transition. The atomic oxygen and nitrogen species concentrations and temperatures obtained from the flow solution at a speed of 5 km/s for an altitude of about 70 km were used to calculate the VUV radiation that would be observed through a rectangular filter with transmission from 122 to 135 nm. The computed in-band radiance was found to be the same as that computed by including only atomic oxygen with a rectangular filter from 129.4 to 131.4 nm. The calculations show that there is an insufficient concentration of atomic nitrogen in the shock layer, for these flight conditions, to contribute to the radiation in the passband of these measurements.

The interpretation of windowless, VUV measurements of the shock-layer radiance could be complicated by absorption of ambient gases and backflow from the shock layer. To avoid these two possibilities the entire payload was hermetically sealed and remained pressurized during the flight. Before launch, the payload was vigorously purged and then positively pressurized with dry argon (Ar). This gas then continued to flow out the small viewing port used for the oxygen VUV measurement, to ensure that the radiation measured had not been attenuated by remaining residual trace species of water, molecular oxygen, or nitric oxide.

The prevention of backflow from the boundary-layer constituents of the shock layer into the viewing port requires that an adequate Ar flow rate be established. The average flow rate of Ar from the main payload (through the tube shown in Fig. 1) into the portion of the payload containing the NO photoionization cell was derived from onboard pressure measurements to be 5.5103×10^{-6} m^3/s (0.7 ft^3/h). Use of that flow rate, the pressure of Ar in the main payload section (1.1445×10^5 N/m^2, 16.6 psia), and the size of the viewing port (9.906×10^{-4} m, 0.039 in. diameter) provides an estimate of the Ar pressure inside the NO photoionization cell chamber region. Estimates of the shock-layer pressure in the vicinity of the instrument were obtained from the flow calculations. It was found that for all altitudes where data were obtained, the ratios of these two pressures were consistent with the Ar purge flow being sonic. Hence, it is unlikely that there was backflow from the shock layer into the NO photoionization cell region, and the planned purged strategy was successful.

Data

Figure 3 shows a summary of the atomic oxygen 130.4-nm radiance data that was obtained during the re-entry portion of the second flight along with the corresponding altitude of the rocket. The atomic oxygen sensor was located 37 deg from the rocket longitudinal axis. The highly oscillatory nature of the signal is due to rocket precession that changes the location of the stagnation point as a function of time during the flight and is more noticeable in the data collected from off-axis sensors. To permit quantitative comparison of data with models, the angle between the sensor and the effective stagnation streamline γ must be known. Using the onboard navigational data supplied by Sandia National Laboratories and transformations of the sensor location into the onboard navigational coordinate reference frame,[3,8] γ can be computed as a function of time. Figure 4 shows an example of radiance correlated with γ during a time region selected at ~75 km. The radiance peaks at small γ (i.e., closer to the stagnation point) and is reduced at the largest values (i.e., towards the wake). The time correlation is sufficiently good to provide information about the radiance angular variation.

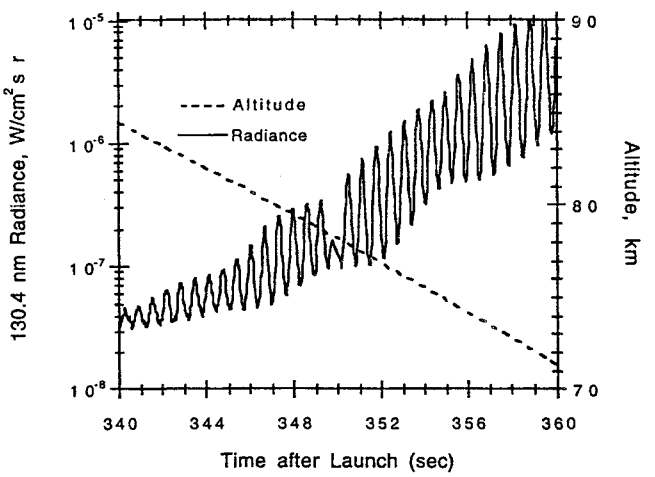

Fig. 3 Atomic oxygen radiance and vehicle altitude as a function of time after launch-re-entry portion of flight.

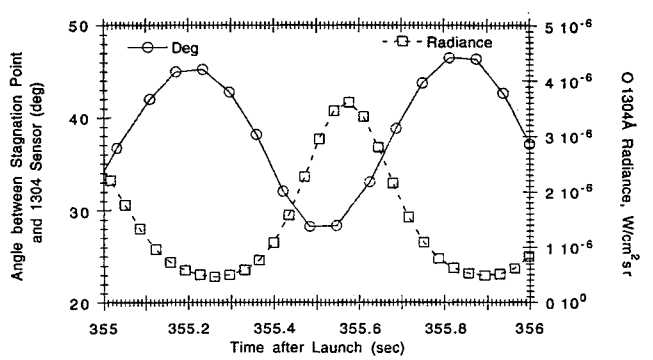

Fig. 4 Comparison of stagnation streamline-sensor angle and VUV radiance as a function of time after launch.

Table 1 Atomic oxygen spectral properties

State number	Term symbol	Degeneracy	Energy level, cm^{-1}
1	^{3}P	9	78
2	^{1}D	5	15,868
3	^{1}S	1	33,792
4	^{5}S	5	73,768
5	^{3}S	3	76,795

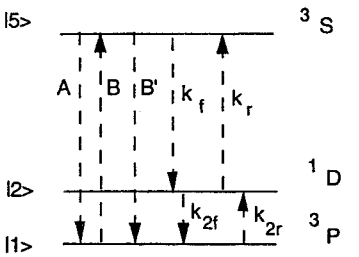

Fig. 5 Three-level atomic oxygen system.

Radiation Model

Modeling of the atomic oxygen 130.4-nm resonance radiation has been considered by Whiting and Park[6] to evaluate heating rates for a blunt body re-entry at 10 km/s. The major excitation processes under these conditions are the electron collisions with O. For the Bow Shock 2 Flight experiment the observed atomic O radiation is due to neutral $-$O collisions. There is an insufficient level of ionization for electron excitation processes to be important. If it is assumed that there are enough collisions such that the electronic states are in a Boltzmann distribution at the heavy particle translational temperature, orders of magnitude more radiation is predicted than was observed. Therefore, a rate equation approach must be considered. A new model is proposed that assumes neutral excitations with O and that the upper state ^{3}S population is obtained from the steady-state solution of the appropriate rate equations.

Table 1 shows the atomic oxygen energy levels for the first five electronic states.[9] Rates for neutral collisional excitations among the first three states have been measured and are high for the temperatures obtained in the shock layer. Therefore, these levels are assumed to be in a Boltzmann distribution at the heavy particle translational temperature. The strongly allowed dipole resonance $^3P \rightarrow {}^3S$ transition is then modeled as the three-level system shown in Fig. 5. In the absence of e^- collisions we assume that collisions of the O(^{1}D) state with neutrals will produce a transition to the ^{3}S state. A measured or calculated O(^{1}D)-neutral collisional excitation rate to the O(^{3}S) state could not be found. Therefore, an estimate for this rate will be used based on data for k_{2r} given in Ref. 10.

The rate equations for this three level system are

$$\frac{d[O(^1D)]}{dt} = k_f[O(^3S)][M] - k_r[O(^1D)][M] - k_{2f}[O(^1D)][M] + k_{2r}[O(^3P)][M] \quad (1)$$

$$\frac{d[O(^3S)]}{dt} = -k_f[O(^3S)][M] + k_r[O(^1D)][M] - A\rho[O(^3S)] \quad (2)$$

where M is a neutral species in the flow other than atomic oxygen (most likely N_2), and A represents the Einstein spontaneous emission coefficient (3.8×10^8 s^{-1}). In Eq. (2) the spontaneous emission coefficient is seen to be multiplied by a unitless factor ρ, whose value is between 1 and 0, and is known as the escape factor. The other rates used in Eqs. (1) and (2) are defined by Fig. 5.

Following the treatment of Athay[11] the escape factor is defined as

$$\rho = 1 - \frac{(B[\mathrm{O}(^3\mathrm{P})] - B'[\mathrm{O}(^3\mathrm{S})])}{A[\mathrm{O}(^3\mathrm{S})]} \times \int J_\nu \Phi_\nu \, d\nu \qquad (3)$$

where B is the absorption rate, and B' is the stimulated emission rate, at the resonance transition and

$$\int J_\nu \Phi_\nu \, d\nu = -\int e^{-\tau_\nu} \Phi_\nu \int_0^{\tau_\nu} S_\nu e^{-s} \, ds \, d\nu \qquad (4)$$

The source function S_ν is defined as

$$S_\nu = \frac{A[\mathrm{O}(^3\mathrm{S})]\Psi_\nu}{(B[\mathrm{O}(^3\mathrm{P})] - B'[\mathrm{O}(^3\mathrm{S})])\Phi_\nu} \qquad (5)$$

with Ψ_ν and Φ_ν defined as the emission and absorption line profiles, respectively, and the index ν represents the frequency of light. Finally, the optical depth (or opacity) τ_ν in Eq. (4) is defined as

$$d\tau_\nu = -h\nu(B[\mathrm{O}(^3\mathrm{P})] - B'[\mathrm{O}(^3\mathrm{S})])\Phi_\nu \, dx \qquad (6)$$

where dx represents a differential length through the shock layer. The radiation I that is observed by the NO photoionization cell represents a spatial integration from the freestream to the body and a spectral integration over the bandwidth of the detector. The spectral integration is straightforward. The spatial integration requires the solution of the classical radiative transport equation, which is given here for completeness:

$$I_\nu = -e^{-\tau_\nu} \int_0^{\tau_\nu} S_\nu e^{s} \, ds \qquad (7)$$

Hence, to obtain the integrated intensity I, the coupled set of Eqs. (1–7) must be solved. We use an approach that has been followed in earlier work; i.e., we accept approximations to Eqs. (5) and (6) given in Refs. 9 and 11 that give a closed form for ρ and permit an approximate solution of Eq. (7). The approximation that Ψ_ν and Φ_ν are equal, hence, S is not a function of ν, simplifies Eqs. (4) and (7). The additional approximation made is that the varying optical depth of the shock layer can be represented by an average quantity, or

$$\tau_0 \approx k_0 \Delta x \qquad (8)$$

where k_0 is the absorption coefficient at the Doppler frequency. The escape factor ρ can then be expressed in closed-form power series expressions of τ_0. It will be seen that it is difficult to choose a priori a value of Δx such that Eq. (8) holds for all locations in the shock layer.

Due to the lack of detailed collisional rate data we make the following assumptions to relate k_f, the quenching rate from the ^{3}S to ^{1}D state, to the k_{2r}, k_{2f}, and k_r excitation rates:

$$k_{2f} = k_f$$
$$k_{2r} = k_{2f}(Q_2/Q_1) \qquad (9)$$
$$k_r = k_{2r}(Q_1 Q_5/Q_2^2)$$

In steady state the derivatives in Eqs. (1) and (2) are set to zero and an expression for the upper state ^{3}S concentration is obtained

$$[\mathrm{O}(^3\mathrm{S})]_{qss} = \frac{[\mathrm{O}(^3\mathrm{P})]n_t k_f}{n_t k_f + A\rho\left(1 + Q_2/Q_5\right)} \cdot \frac{Q_5}{Q_1} \qquad (10)$$

where n_t is the total number density in the flow and Q_i is the partition function of the ith state (Table 1).

Equation (10) predicts a density functional form for the 130.4-nm radiation. In the limit of a sufficiently high collision rate, i.e., $n_t k_f >> \rho A$, the ^{3}S population is given by the Boltzmann distribution. The low collision rate limit of Eq. (10)

$$[\mathrm{O}(^3\mathrm{S})]_{qss} \approx \frac{[\mathrm{O}(^3\mathrm{P})]n_t k_f}{A\rho} \cdot \frac{Q_5}{Q_1}, \qquad n_t k_f << A\rho \qquad (11)$$

predicts a different functional form for the 130.4-nm radiation. In earlier work it has been shown that the production of atomic oxygen is second-order in n_t.[2,4] Hence, Eq. (11) predicts that the atomic oxygen radiation should be proportional to n_t^3. To test this hypothesis the density dependence of the data was examined. Figure 6 shows data taken at altitudes between 80–70 km for measurements at an angle of 36 ± 0.2 deg from the stagnation streamline. Given for comparison are different power laws in n_t. The third law power in n_t can be seen to give a much better fit than a square or fourth-order variation. The data suggest that the collision rates are not high enough to establish a Boltzmann distribution. This is similar to what was observed for the NO 230-nm radiation from the second flight data.

It is instructive to compare the density dependence of the O radiation at 130.4 nm with the NO 230-nm radiation mea-

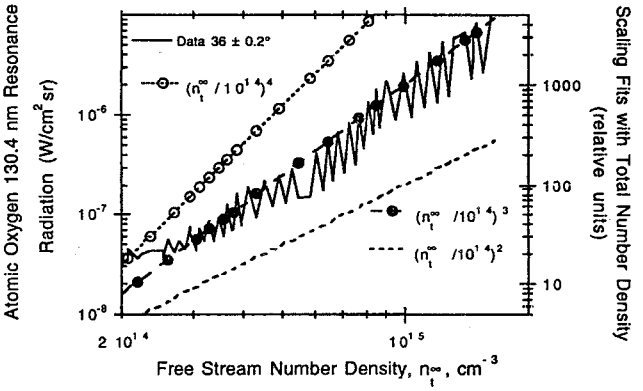

Fig. 6 Comparison of atomic oxygen data and density dependence.

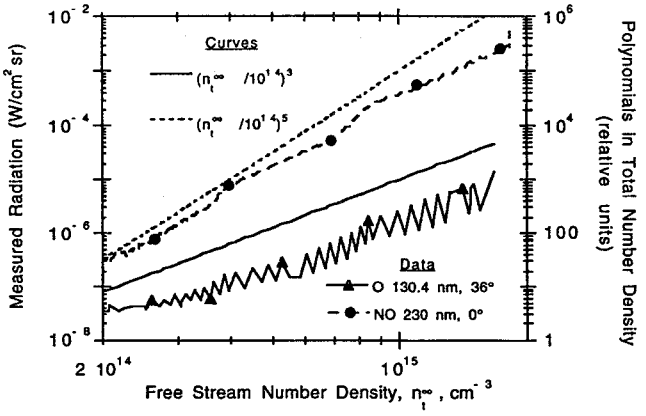

Fig. 7 Comparison of freestream density dependence of atomic oxygen-VUV and NO-UV data.

surements. First, the chemical production mechanisms for O are second-order in n_e, compared to third-order for NO.[2,4] Second, the spontaneous emission rate for the O 130.4 nm is about a factor of 100 greater than that for the NO 230-nm radiation. Hence, it is expected that the two sets of data should exhibit a different density dependence. Figure 7 shows a comparison of the two data sets as a function of freestream number density as well as different power curves. The different density dependence observed is consistent with the above arguments.

Calculations

The computational technique that has been used to simulate the stagnation region flowfield is that given in Refs. 2 and 4, which discusses enhancements to the original flow modeling of Candler and MacCormack.[12] Briefly, the shock-heated air is modeled by eight chemical species (N_2, O_2, NO, NO^+, N_2^+, N, O, and e^-) that are allowed to react with each other at finite rates. Three independent temperatures in the flow are modeled: 1) heavy particle translational, 2) molecular rotational, and 3) a combined molecular vibrational and electron translational temperatures. The spherical nose of BSUV-2 was represented with a 56 × 100 body-fitted grid. The size of the grid normal to the surface was adjusted depending on the computed shock-layer thickness. With convergence studies, we found this grid dimension to be sufficient. The atomic oxygen concentration and heavy particle temperature obtained at each point in the flow have been used to compute the 130.4-nm radiation. Figures 8 and 9 show shock-layer profiles as a function of altitude that were used in the radiation calculations. The profiles are shown along a radial close to 36 deg from the freestream to the wall (or surface), as is shown in the Fig. 1 insert. The calculated atomic oxygen number density is seen to vary by about five orders of magnitudes over the altitude range to be compared with data. The heavy particle translational temperature, however, is fairly constant (as is consistent for a constant velocity). The excited state population [given by Eq. (10)] is therefore sensitive to the

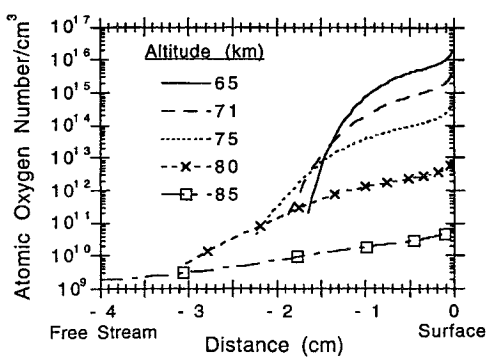

Fig. 8 Comparison of calculated atomic oxygen number density shock-layer profiles as a function of altitude.

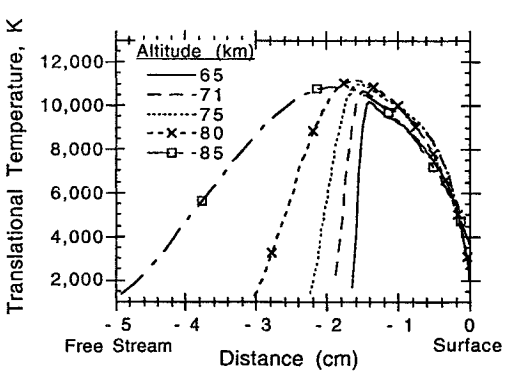

Fig. 9 Comparison of calculated heavy particle temperature shock-layer profiles as a function of altitude.

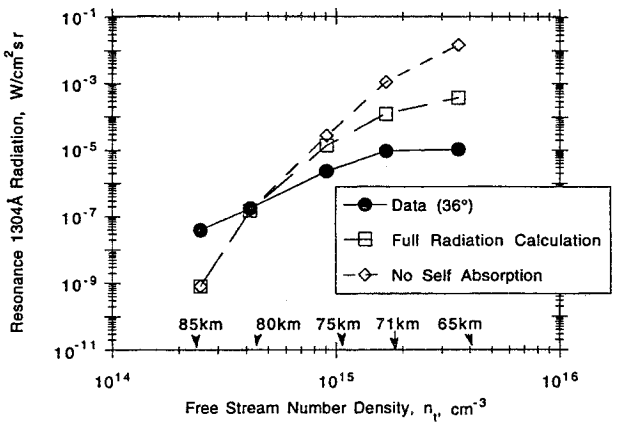

Fig. 10 Comparison of new NEQAIR 2 calculations with data.

accuracy of the shock-layer chemistry modeling as a function of shock-layer density (or altitude).

Equation (10) has been incorporated into the NEQAIR 2 model. The calculations have modeled the dependence of the upper state population on absorption processes through the use of the escape factor. The radiative transport capability of the NEQAIR model has been used to evaluate 130.4-nm radiation at altitudes of 85, 80, 75, 71, and 65 km with the flow solutions. A value of k_f of 8×10^{-11} cm³/s at 300 K obtained from Ref. 10 was used. A measurement of the quenching coefficient is needed; however, by the previously mentioned arguments its value should be fairly constant over the altitude range considered here. Hence, if the radiation model is correct, the shape of the predicted radiance should be in agreement with the data.

Figure 10 shows the results of the calculations for the radiance at the body (i.e., the location of the 130.4 sensor) and the data, both at 36 deg from the rocket axis. The corresponding altitudes are also indicated. The calculations labeled "no self absorption" were performed by setting all absorption rates to zero. Comparison of these results with the full calculation serves to indicate the degree of shock-layer optical thickness. The comparison of theory and data can be seen to subdivide into the "high altitude" and "low altitude" cases.

At altitudes where the shock layer is predicted to be optically thin (i.e., higher than 75 km) the calculations do not predict the correct radiation density dependence. At the highest altitude, the data is approaching the shot noise limit that makes it difficult to correlate exactly the sensor viewing location as a function of time in the precession period. These errors, however, are probably small in comparison to the difference observed with theory. Theory is seen to fall off faster than experiment. This is consistent with the comparisons presented in Ref. 4 between the predicted and measured NO 230-nm spectral and in-band radiance. Therefore, the thermochemical modeling of atomic oxygen concentration should also be further examined.

The comparison of the calculations labeled no self absorption with "full radiation" indicate the greater opacity of the shock layer at altitudes lower than 75 km. Comparison with the data show, as expected, that inclusion of self-absorption is important. The full radiation calculation, however, is still more than an order of magnitude higher than the data at 65 km and does not show the same leveling-off in the in-band radiance as the data does. Measurements have been made of atomic oxygen resonance radiation generated in the NASA Ames electric arc-driven shock-tube facility, under conditions similar to the flight data. Comparison of those measurements with modeling also showed the computations to overpredict the data.[5]

The disagreement between theory and data for the higher density cases is most likely due to remaining inadequacies in the radiation modeling. Since the boundary layer is optically

thick the radiance at the body should be relatively insensitive to uncertainties of the computed flow atomic oxygen concentration and temperature in the shock layer. Therefore to emphasize the aspects of the radiation modeling that may be deficient, consider the basic components of the radiation calculation at 65 km as shown in Fig. 11. The two rates given in Eq. (10), $k_f n_t$ and ρA, and the excited state O(^{3}S) population are shown along the 36-deg radial (see Fig. 1 insert). The figure shows that for this case both collisional quenching and radiative decay are important. Examination of these rate profiles for the higher altitude cases showed that the radiative decay rate $A\rho$ dominates. For these cases, unlike the result at 65 km, the escape factor spatial profile $\rho(x)$ was computed to be approximately unity over most of the shock-layer. The results shown in Fig. 11 are input to the radiative transport equation [Eq. (7)]. Figure 12 shows the components of Eq. (7), the shock-layer profiles of the emissive power, the absorption coefficient, and the cumulative intensity integrated from the freestream towards the body (designated as surface intensity) at 65 km. It is clear that there is no spatial portion of the shock layer where both the emission and absorption are uniform. The asymmetry in the shock-layer optical thickness is also apparent from the absorption coefficient profile and the surface intensity. Hence, the assumption of a constant escape factor is not valid.

Two simple changes to the radiation model that might provide better agreement between theory and data at altitudes $\leq$75 km are to change the quenching rate k_f, or the escape factor ρ. A reasonable change of k_f would be to assume smaller values than used here. Since the maximum shock-layer temperatures are nearly constant for the altitudes of interest, changes in k_f would change the magnitude of the "full radiation calculation" curve shown in Fig. 10, but not the shape. This can be seen in Fig. 13. Hence, a change in k_f by a factor

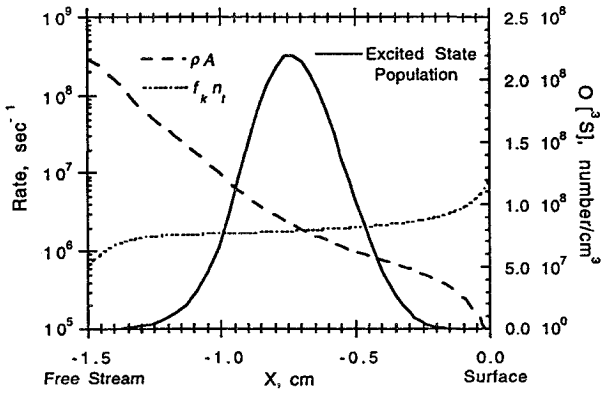

Fig. 11 Calculated excitation rates and excited state population shock-layer profiles at 65 km.

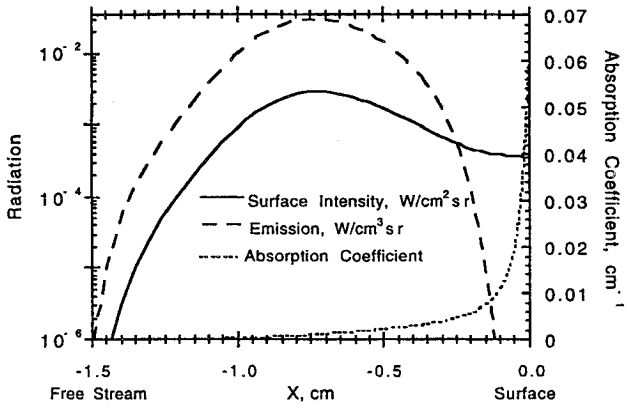

Fig. 12 Calculated radiance and absorption shock-layer profiles at 65 km.

$\approx$10 is probably not sufficient to account for the entire discrepancy.

As mentioned earlier, there are assumptions in the present modeling of the escape factor that may require changes in the way that term is presently computed. The key assumptions of Refs. 9 and 11 that are used to give a closed form solution of Eq. (10) are that there is a uniform, isotropic radiating portion of the shock layer and that the absorption and emission line shape profiles are the same. Figure 12 shows that the assumption of spatial uniformity may be incorrect. To obtain a closed form for the escape factor it is also required that a depth Δx be chosen that gives a representative "average optical depth" in the shock layer. The present calculations have assumed that Δx = 1 cm. Further modeling may be required to replace this "average" treatment with one that takes into account the spatial variability of the radiation field and its influence on the population of the excited state. Such modeling, however, is beyond the scope of this article.

To assess the potential impact of changes to the escape factor formalism for the higher density cases, ρ was set equal to its maximum possible value, 1. Figure 13 shows a comparison of the data, the baseline (full radiation) calculation of Fig. 10, and the results with ρ = 1. For this last calculation, it should be emphasized that the varying optical thickness and self-absorption in the boundary layer is still accounted for in the radiative transport portion of the calculation. The agreement between the density dependence of the lower altitude radiance calculations and the data improves with this change. Figure 14 shows another type of comparison of data and modeling. Detailed comparison of the data and radiation modeling is shown as a function of angle from the stagnation streamline

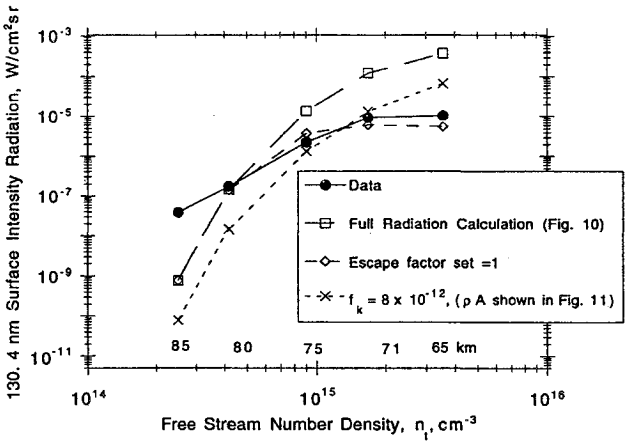

Fig. 13 Comparison of changes in baseline radiation rates with data.

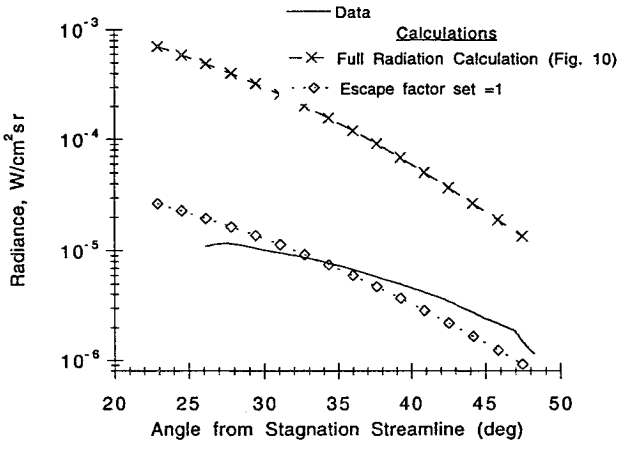

Fig. 14 Comparison of data and radiation modeling as a function of angle from the stagnation streamline and the sensor at ~71 km.

at an altitude of about 71 km. For this comparison the total number density remains almost constant; but, the temperature changes. The baseline radiation calculation is seen to vary in shape and absolute magnitude from the data. The baseline model was changed by setting the escape factor to 1 as in Fig. 13. The absolute magnitude is in better agreement with the data and the angular dependence improves somewhat. Taking the results shown in Figs. 13 and 14, we conclude that the improved agreement with the data seem to indicate that a sufficient number of the emitted photons can reduce the upper state population through radiation.

Conclusions

Atomic oxygen 130.4-nm data from the NO-filled, CaF_2 window ionization chamber has been analyzed from the second Bow Shock Ultra Violet Flight Experiment. The data have been correlated with time, altitude, and angle between the stagnation streamline and the ionization cell FOV. The data thus provide a new source of VUV radiance measurements collected under flight environmental conditions.

An excitation model has been proposed which makes two key assumptions: 1) neutral species collisional excitations of atomic oxygen are the source of 130.4-nm resonance radiation and 2) an escape factor is used to model the reduction of the excited state population through photon emission. The data encompasses a flight regime where both contributions are important.

Self-absorption has been included in the calculations shown here, but, replacement of the approximate escape factor formalism with a self-consistent treatment of the radiation field will be considered for future work. This level of treatment is required to assess whether the difficulty with the present approximate escape factor is numerical or if additional important physical processes are missing. The calculations shown here with the escape factor set to one provide a useful bound. The significant improvement of theory with data suggests that when the photon processes are rigorously modeled it will be found that photons are able to escape from the optically thick medium. The enhanced understanding of photon escape processes will improve the modeling of other atomic resonant transitions as well.

The atomic oxygen radiance calculations and data do not show the same dependence on density at altitudes above 80 km. This condition is similar to the observations of NO radiation in the 230-nm spectral region, as reported earlier.[4] The disagreement between data and theory is attributed to inadequacies in the flow modeling, and not the radiation model. For this portion of the flight data, the modeling of the escape factor is not an issue; ρ is equal to 1 since the flow is optically thin. The flow thermochemical modeling of the atomic oxygen kinetics therefore requires further study. Since atomic oxygen is a precursor to the formation of NO, the data offer a rigorous test for future thermochemical models.[13]

Acknowledgments

This research is supported by the BMDO/IST and managed in part by the Army Research Office under Contract MDA903-89-C-0003.

References

[1]Erdman, P. W., Zipf, E. C., Espy, P. J., Howlett, C., Levin, D. A., Loda, R., Collins, R. J., and Candler, G. V., "Flight Measurements of Low Velocity Bow Shock Ultraviolet Radiation," *Journal of Thermophysics and Heat Transfer*, Vol. 7, No. 1, 1993, pp. 37–41.

[2]Levin, D. A., Candler, G. V., Collins, R. J., Erdman, P. W., Zipf, E. C., Espy, P. J., and Howlett, C., "Comparison of Theory with Experiment for the Bow Shock Ultraviolet Rocket Flight," *Journal of Thermophysics and Heat Transfer*, Vol. 7, No. 1, 1993, pp. 30–36.

[3]Erdman, P., Zipf, E., Howlett, C., Levin, D., Candler, G., and Collins, R., "Measurements of Ultraviolet Radiation from a 5 km/s Bow Shock," *Journal of Thermophysics and Heat Transfer*, Vol. 8, No. 3, 1994, pp. 441–446.

[4]Levin, D., Candler, G., Collins, R., Erdman, P., Zipf, E., and Howlett, C., "Examination of Theory for Ultraviolet Rocket Experiments—I," *Journal of Thermophysics and Heat Transfer*, Vol. 8, No. 3, 1994, pp. 447–452.

[5]Sharma, S. P., and Whiting, E. E., "Modeling of Nonequilibrium Radiation Phenomena: An Assessment," AIAA Paper 94-0253, Jan. 1994.

[6]Whiting, E. E., "Radiative Heating at the Stagnation Point of the AFE Vehicle," NASA TM 102829, 1990.

[7]Samson, J. A. R., *Techniques of Vacuum Ultraviolet Spectroscopy*, Pied Publications, ISBN 0-918626-15-3, Lincoln, NE, 1967.

[8]Rollstin, L., private communication, Sandia National Labs., Albuquerque, NM.

[9]Park, C., *Nonequilibrium Hypersonic Aerothermodynamics*, Wiley, ISBN 0-471-51093-9, New York, 1990.

[10]Bortner, M. H., Bauer, T., and Blank, C. A., "DNA Reaction Rate Handbook," Rept. DNA 1948H, March 1972.

[11]Athay, R. G., *Radiation Transport in Spectral Lines*, D. Reidel Publishing Co., ISBN 90 277 0228 4, Holland, 1972.

[12]Candler, G. V., and MacCormack, R. W., "Computation of Hypersonic Ionized Flows in Chemical and Thermal Nonequilibrium," *Journal of Thermophysics and Heat Transfer*, Vol. 5, No. 3, 1991, pp. 266–273.

[13]Boyd, I. D., Candler, G. V., and Levin, D. A., "Dissociation Modeling in Low Density Hypersonic Flows of Air," *Physics of Fluids* (to be published).